# Properties of the intrinsic surface of liquid acetone, as seen from computer simulations

Pál Jedlovszky,[1,2,3,*] Balázs Jójárt,[4] and George Horvai[2,5]

[1]*Laboratory of Interfaces and Nanosize Systems, Institute of Chemistry, Eötvös Loránd University, Pázmány P. Stny 1/A, H-1117 Budapest, Hungary*

[2]*MTA-BME Research Group of Technical Analytical Chemistry, Szt. Gellért tér 4, H-1111 Budapest, Hungary*

[3]*EKF Department of Chemistry, Leányka utca 6, H-3300 Eger, Hungary*

[4]*Department of Chemical Informatics, Faculty of Education, University of Szeged, Boldogasszony sgt. 6. H-6725 Szeged, Hungary*

[5]*Department of Inorganic and Analytical Chemistry, Budapest University of Technology and Economics, Szt. Gellért tér 4, H-1111 Budapest, Hungary*

**Running title:** Intrinsic Surface of Liquid Acetone

[*]Electronic mail: pali@chem.elte.hu

**Abstract**

Molecular dynamics simulations of the liquid-vapour interface of acetone have been performed in the canonical ($N$,$V$,$T$) ensemble at 298 K with two different molecular models, belonging to the TraPPE and CHARMM27 force fields, respectively. The first three molecular layers of the liquid phase beneath its surface have been identified by means of the Identification of the Truly Interfacial Molecules (ITIM) method. The results obtained reveal that the vicinity of the vapour phase affects only the first molecular layer of the liquid phase, and its effect vanishes in every respect already in the second molecular layer. The surface acetone molecules exhibit a dual orientational preference. In their dominant orientation the molecules stay perpendicular to the macroscopic plane of the liquid surface, the C=O bond lying almost parallel, whilst the line connecting the two $CH_3$ groups staying almost perpendicular to this plane, declining only by about $5^o$ from the perfectly parallel and perpendicular alignments, respectively. This finding is also in a clear accordance with results of some of the former experimental studies of this system. Besides the above orientation, another alignment is also found to be preferred, in particular, at the tips of the crests of the molecularly wavy liquid surface. In this orientation, the acetone molecule lays almost parallel with the surface plane, declining by about $10^o$ from it, pointing the O atom slightly toward the liquid, whilst the two $CH_3$ groups slightly toward the vapour phase

## 1. Introduction

Acetone is one of the most widely used polar solvents both in preparative organic chemistry and in the chemical industry. Acetone is a prototypical example of strongly dipolar but yet aprotic molecules. As a consequence, liquid acetone is characterized by rather high boiling point and dielectric constant, but by considerably lower surface tension and heat of evaporation values than hydrogen bonding liquids of similar mass. Further, as a potential H-acceptor, acetone is miscible in any ratio with water as well as other hydrogen bonding liquids, such as small alcohols. Because of its importance the properties of acetone have been investigated in detail in different systems by a variety of experimental methods [1-12], and these investigations were well complemented by numerous computer simulation studies of neat bulk liquid acetone [13-17], mixtures of acetone in various proportions with water [18-27], with other solvents [28-33] and solvent mixtures [34], adsorption layer of acetone at the surface of ice [35,36], and aqueous acetone nanoclusters [37].

Much less effort has, however, been expended on the investigation of the liquid-vapour interface of acetone and aqueous acetone mixtures. Simulation of the latter systems was severely hindered by the fact that the first acetone model that reproduces the full miscibility with water [26] has only been proposed recently [25]. The molecular level properties of the liquid-vapour interface of neat acetone were first studied in the pioneering work of Yeh et al. both by vibrational sum frequency generation (SFG) spectroscopy and molecular dynamics computer simulation [7]. They found that the surface acetone molecules, similarly to those in the planar layers present in the crystalline phase, prefer the orientation in which the line connecting the two $CH_3$ groups is perpendicular to the interface [7]. In a subsequent SFG study using the polarization null angle method [38,39] Chen et al. found a slightly different orientational preference of the acetone molecules, in which one of the C-$CH_3$ bonds stays perpendicular to the liquid surface [10]. The preference for this orientation was later confirmed by computer simulation [40], although the strength of this preference was found to be considerably smaller [40] than what was assumed by Chen et al. [10]. Using bivariate orientational analysis [41,42] in computer simulation another preferred surface orientation, in which the line joining the two $CH_3$ groups lays parallel with the surface and the C=O bond points flatly inward, was also detected [40]. The observed dual surface orientational preference was in a clear accordance with what was later found in the adsorption layer of acetone at the surface of ice [36].

Both of the computer simulation studies reported on the liquid-vapour interface of neat acetone so far [7,40] suffer, however, from the problem of inadequately locating the liquid surface itself. The problem originates from the fact that liquid surfaces are not flat on the molecular scale, but are corrugated by capillary waves, the amplitude of which being at last in the order of molecular size. Due to the presence of these capillary waves the detection of the exact position of the liquid surface, or, equivalently, the detection of the full set of molecules that are right at the liquid surface (i.e., at the boundary of the liquid and vapour phases) is not a simple task at all. On the other hand, the neglect of these capillary waves in the analysis, and the use of a slab parallel with the Gibbs dividing surface as the 'surface layer', as done in both previous simulations of the acetone surface [7,40] and in numerous studies of other liquid surfaces, leads to the misidentification of a large set of molecules. Thus, a large number of molecules that are surrounded by like neighbours in all directions are incorrectly identified as 'interfacial' ones, and also many molecules that are at the boundary of the two phases are wrongly identified as 'non-interfacial ones' this way [43-48]. This misidentification results in a systematic error not only in the structural properties of the interface [43-47], but also in the calculated thermodynamic properties of the system studied [48].

The need for using the real, capillary wave corrugated intrinsic surface of a liquid phase in analysing results of computer simulations was realized about a decade ago. Since then, following the pioneering work of Chacón and Tarazona [49] a number of methods that are able to locate the intrinsic surface have been proposed [43,49-55], among which the Identification of the Truly Interfacial Molecules (ITIM) [43] turned out to be an excellent compromise between computational cost and accuracy [54]. In the ITIM analysis spherical test particles of appropriate size are moved from the bulk opposite phase to the surface along a set of test lines perpendicular to the macroscopic plane of the surface. Each test sphere stops when it touches the first molecule of the phase of interest, and the molecules that stopped the probe along at least one test line are regarded as being at the interface (as they are 'seen' by the probe from the opposite phase) [43].

In this paper we present a thorough analysis of the intrinsic surface of liquid acetone. The computer simulation results are analyzed in terms of the ITIM method. To avoid any arbitrariness of the results due to the particular choice of the force field used, we repeated all the calculations using two different potential models of acetone, i.e., a four site one belonging to the TraPPE force field, which describes the $CH_3$ groups as united atoms [29], and a ten site one using all-atom representation, which belongs to the CHARMM27 force field [56]. These models differ considerably in their dipole moment values: whilst the TraPPE model

4

corresponds to the dipole moment of 2.50 D, in accordance with the majority of the acetone potentials as well as with the experimental gas phase value of 2.88 D, [57,58] the CHARMM27 model takes polarization effect into account in an average way, having a molecular dipole moment of 3.68 D. Besides the surface orientation of the molecules we address here questions concerning the separation and width of the subsequent subsurface molecular layers, molecular scale roughness of the liquid surface, dynamics of exchange of the molecules between the surface layer and the bulk phase, and the extent, in terms of molecular layers, to which the vicinity of the vapour phase influences the properties of liquid acetone.

The paper is organized as follows. Details of the molecular dynamics simulations and ITIM analyses performed are given in section 2. The obtained results are presented and discussed in detail in section 3, while in section 4 the main conclusions of this study are summarized.

## 2. Computational details

Molecular dynamics simulations of the liquid-vapour interface of acetone have been performed on the canonical ($N,V,T$) ensemble at 298 K, employing two acetone potential models that belong to the TraPPE [29] and CHARMM27 [56] force fields. The TraPPE model treats the $CH_3$ groups as united atoms, whilst the CHARMM27 model uses all-atom representation. The TraPPE acetone model is shown to excellently reproduce the thermodynamic properties of liquid acetone [29] and, e.g., acetone-methanol mixtures [33], whereas the CHARMM27 potential provides the basis of a simple polarizable model, developed specifically for acetone-water mixtures [25], which is currently the only acetone model shown to reproduce the full miscibility with water [26].

Both acetone models describe the interaction energy of two molecules as the sum of the Lennard-Jones and charge-charge Coulomb contributions of all their atomic pairs. Thus, the interaction energy of molecules $i$ and $j$ is calculated as

$$u_{ij} = \sum_{\alpha=1}^{n_s} \sum_{\beta=1}^{n_s} \frac{1}{4\pi \in_0} \frac{q_\alpha q_\beta}{r_{i\alpha,j\beta}} + 4\varepsilon_{\alpha\beta}\left[\left(\frac{\sigma_{\alpha\beta}}{r_{i\alpha,j\beta}}\right)^{12} - \left(\frac{\sigma_{\alpha\beta}}{r_{i\alpha,j\beta}}\right)^6\right], \tag{1}$$

and the total potential energy of the system is simply the sum of the interaction energies of all molecule pairs. In the above equation indices $\alpha$ and $\beta$ run over all the $n_s$ interaction sites of molecules $i$ and $j$, respectively, $r_{i\alpha,j\beta}$ is the distance of site $\alpha$ of molecule $i$ from site $\beta$ of molecule $j$, $q_\alpha$ and $q_\beta$ are the fractional charges carried by the respective interaction sites, $\varepsilon_{ab}$ and $\sigma_{ab}$ are the Lennard-Jones energy and distance parameters, respectively, and $\in_0$ is the vacuum permittivity. The Lennard-Jones parameters corresponding to the site pair $\alpha$ and $\beta$ are derived from the values characteristic to the single interaction sites by the Lorentz-Berthelot rule [59], i.e.,

$$\sigma_{AB} = \frac{\sigma_A + \sigma_B}{2} \tag{2}$$

and

$$\varepsilon_{AB} = \sqrt{\varepsilon_A \varepsilon_B} \; . \tag{3}$$

The interaction parameters of the two acetone models considered are summarised in Table 1.

The acetone molecules have been kept rigid in the simulations, their bond lengths and bond angles have been fixed to their equilibrium values by means of the LINCS algorithm [60]. The bond length and bond angle values of the two models considered are collected in Table 2.

The simulations have been performed by the GROMACS 4.5.5 program package [61]. In both cases 4000 acetone molecules have been placed into the rectangular basic simulation box, the $X$, $Y$, and $Z$ edges of which have been 200, 70 and 70 Å, respectively, in the case of the TraPPE, and 400, 50 and 50 Å, respectively, in the case of the CHARMM27 simulation, $X$ being the axis perpendicular to the macroscopic liquid surface. Standard periodic boundary conditions have been applied, and all interactions have been truncated to zero beyond the centre-centre based cut-off distance of 15 Å. The long range part of the electrostatic interaction has been accounted for by the Particle Mesh Ewald (PME) method [62]. The equations of motion have been integrated in time steps of 2 fs. The temperature of the system has been controlled by the Nosé-Hoover thermostat [63,64] in the case of the TraPPE, and by the Berendsen thermostat [65] in the case of the CHARMM27 simulation.

Initial configurations have been generated by placing the required number of molecules in a rectangular basic box, the $Y$ and $Z$ edges of which have already been set to their final values, whereas the length of the $X$ edge has roughly corresponded to the density of liquid acetone. After proper energy minimisation the systems have been equilibrated for 1 ns

on the isothermal-isobaric ($N,p,T$) ensemble at 1 bar in such a way that only the $X$ axis of the basic box has been allowed to change. Then the interfacial systems have been created by increasing the $X$ edge of the basic box to its final value. The interfacial systems have further been equilibrated on the canonical ensemble for 2 ns. Then, in a 2 ns long production stage 2000 sample configurations per system, separated from each other by 1 ps long trajectories each, have been saved for further analyses.

The interfacial layer of the acetone molecules as well as the molecules constituting the second and third subsurface layers have been identified by means of the ITIM method [43]. Test lines parallel with the macroscopic interface normal axis $X$ have been arranged in a square-like grid with a spacing of the neighbouring lines of 0.5 Å. The radius of the spherical probe has been 2 Å, in order to ensure that it is in the size range of the atoms [43,54]. The size of the various atoms of the acetone molecules has been approximated by their Lennard-Jones distance parameter, $\sigma$. The molecules constituting the second and third subsurface layers have been identified by disregarding the molecules already identified as belonging to the previous layer(s), and repeating the entire ITIM procedure on the remainder of the system. The first three layers of acetone beneath the liquid-vapour interface are shown in Figure 1, together with the bulk liquid phase, as identified in an equilibrium snapshot of the TraPPE system. Finally, all calculated quantities have been averaged over the 2000 sample configurations, including both liquid-vapour interfaces present in the basic simulation box.

## 3. Results and Discussion

First, we have calculated the surface tension, $\gamma$, of acetone in both of the systems simulated. Its value is resulted in 22.9 mN/m using the TraPPE potential, in an excellent agreement with the experimental value of 23.3 mN/m [66]. The surface tension of the CHARMM27 system of 19.0 mN/m turned out to be also in a reasonable agreement with the experimental value.

### 3.1. Density profiles

The number density profile of acetone molecules along the macroscopic interface normal axis $X$ is shown in Figure 2 as obtained in the two systems simulated. The number density profiles of molecules constituting the first three molecular layers beneath the surface are also indicated.

The profiles obtained with the two potential models are very similar to each other. These profiles clearly emphasize the importance of using an intrinsic method in detecting and analysing the surface of liquid acetone. As is seen, the density peak of the molecules constituting the first layer of the liquid phase extends well into the $X$ range where the density of the system is already equal to the bulk liquid phase density, whereas the second and even the third molecular layer gives a non-negligible contribution in the $X$ range where the density of the system is between the values characteristic of the two bulk phases. Therefore, identifying the interfacial region in the conventional, non-intrinsic way, i.e., by the $X$ range of intermediate densities, would lead to a serious systematic error of any surface analysis, as a large fraction of the molecules would be misidentified regarding their position relative to the interface.

It is also seen that the profiles corresponding to the individual molecular layers can be very well fitted by Gaussian functions. Since the distribution of these molecules along the macroscopic surface normal axis is indeed expected to follow a Gaussian function [67], this finding confirms the proper choice for the radius of the spherical probe used in the ITIM procedure [54,67].

The width parameter of the fitted Gaussian function (i.e., width at half maximum), $\delta$, can serve as a measure of the broadness of the corresponding molecular layer, whereas the difference of the Gaussian peak positions, $X_{\text{peak}}$, of two consecutive layers indicates how closely these layers are packed together. From the values of the surface tension, $\gamma$, and $\delta$ one can also extract the size-independent measure of intrinsic layering, $A_{\text{cut}}$, as $A_{\text{cut}} = YZ \exp(-k_{\text{B}}T \ln 2 / 2\pi\gamma\delta^2)$. The value of $A_{\text{cut}}$ turned out to be $4.64 \times 10^3$ Å and $2.34 \times 10^3$ Å for the first layer of the TraPPE and CHARMM27 systems, respectively. The $\delta$ and $X_{\text{peak}}$ values of the fitted Gaussian functions are summarised in Table 3. As is seen, the first layer is noticeably, by about 4-4.5% and 6-7% broader than the second and third layer, respectively, and the second layer is still, by about 2% broader than the third one. Correspondingly, the separation of the density peaks of the first and second layer, being 5.40 Å and 5.41 Å in the TraPPE and CHARMM27 systems, respectively, is about 2% larger than that of the second and third layers. All these results show that upon approaching the liquid surface the packing of the acetone molecules becomes less tight than in the bulk liquid phase. Similar, but even stronger effect was previously seen at the surface of liquid water [46], whereas no such loosening of the packing of the molecules was observed at the vicinity of the liquid surface of dimethyl sulphoxide (DMSO) [68]. The observed less tight packing of the molecules at the

interface is likely a consequence of their preferred interfacial orientation, which might not be fully compatible with the closely packed arrangement of the bulk liquid phase. This point is further investigated in a following subsection.

### *3.2. Surface roughness*

Having the intrinsic, molecularly rugged surface of the liquid phase already identified, its molecular level roughness can also be analysed in computer simulation. However, the roughness of the liquid surface requires the use of at least two independent parameters, i.e., an amplitude-like and a frequency-like one. Previously we proposed to use the parameter pair $a$ and $\xi$, determined by fitting the function

$$\overline{d}(l) = \frac{a\xi l}{a + \xi l} \tag{4}$$

to the simulated data, as the amplitude-like and frequency-like roughness parameters, respectively [69]. In the above equation $l$ is the lateral distance (i.e., distance in the macroscopic plane of the surface, $YZ$) of two surface points, whilst $\overline{d}$ is the mean distance of two surface points, the lateral distance of which is $l$, along the macroscopic surface normal axis, $X$. Recently we have demonstrated the physical relevance of this description by showing the close relationship between the amplitude-like roughness parameter, $a$, and the surface tension of the system [70].

The $\overline{d}(l)$ roughness curves obtained in the first three molecular layers of the two systems simulated, together with the curves fitted to the first layer data are shown in Figure 3, whereas the values of the $a$ and $\xi$ parameters are included in Table 3. As is seen, both of the roughness parameters are always slightly, by 2-5% larger for the CHARMM27 than for the TraPPE model. This fact is probably simply related to the different description of the methyl H atoms in the two models: contrary to the all-atom CHARMM27 model, the united atom treatment of the $CH_3$ groups in the TraPPE model causes a slight artificial smoothening of the molecular shape, and hence also that of the liquid surface. Further, the fact that the cross section of the two systems in the macroscopic plane of the surface, $YZ$, has been different, leading to a somewhat different range of the allowed capillary waves in the two cases, might also contribute to this difference. It is also seen that the first layer in both systems is found to be somewhat rougher, both in terms of frequency and amplitude than the subsequent ones, whereas the roughness of the second and third layers are much closer to each other, the

second layer being slightly still rougher. Similar, and even stronger increase of the roughness of the first subsurface molecular layer with respect to the subsequent ones was previously observed at the surface of liquid water [46], whereas no change of the layer roughness upon going farther from the interface was seen at the surface of liquid DMSO [68]. Considering the marked orientational structure of the surface layer (but lack of such structure already in the second layer) of water [46], and the lack of marked orientational preferences at the surface of DMSO [68], the present results suggest again that the surface acetone molecules might have rather strong orientational preferences relative to the interface. This point is analysed in detail in a following subsection.

### 3.3. Dynamics of exchange between the surface layer and the bulk liquid phase

The dynamics of exchange of the molecules between the interfacial layer and the bulk liquid phase can be characterised by the survival probability and mean residence time of the molecules at the surface. The survival probability $L(t)$ is simply the probability that a molecule that belongs to the surface layer at $t_0$ remains at the surface up to $t_0+t$. In order to distinguish between the situations when (i) a molecule only leaves the surface layer due to some oscillation, and returns immediately back, or (ii) it leaves the surface layer permanently, departure of the molecules is allowed in the time interval between $t_0$ and $t_0+t$, given that the molecule returns to the surface layer within $\Delta t$. Here we have used two different $\Delta t$ values, namely 1 ps and 2 ps. The survival probabilities obtained with $\Delta t = 1$ ps and $\Delta t = 2$ ps are referred here as 'continuous' and 'intermittent' survival probabilities, respectively, since the $\Delta t$ time window of 1 ps equals the trajectory length between two saved configurations. In other words, when using the $\Delta t = 1$ ps time window an acetone molecule is considered to have left the surface if it is not found in the surface layer in any single sample configuration. On the other hand, in the case of $\Delta t = 2$ ps a molecule can be missing from the surface layer in a sample configuration, given that it is back to the surface in the next one.

The continuous and intermittent survival probabilities calculated in the first three molecular layers of the two systems simulated are shown in Figure 4. Since the process that a molecule leaves the surface layer is of first order kinetics, the obtained $L(t)$ curves can be very well fitted by exponentially decaying functions. To emphasize this exponentially decaying character of the survival probability, Fig. 4 shows the obtained $L(t)$ data on a logarithmic scale. Fitting the function $\exp(-t/\tau)$ to the calculated $L(t)$ data provides the mean residence time of the molecules at the surface (or in a subsequent subsurface layer), $\tau$. The $\tau$ values

10

obtained for the first three molecular layers of the two systems simulated are collected in Table 3.

As is seen, the two models have again given rather similar results. The continuous and intermittent residence time values in the first layer are around 16.5 and 28 ps, respectively. These values are rather similar to those obtained at the surface of liquid DMSO [68], but are considerably (i.e., by a factor of 2-4) larger than those obtained at the surface of neat water [44,46] and neat methanol [44], reflecting the slower diffusion of acetone or DMSO than water and methanol.

It is also seen that the $\tau$ values obtained in the second and third molecular layers beneath the surface are always very close to the $\Delta t$ time window used in the calculation, indicating that the exchange of the molecules between these layers and the rest of the system occurs on a considerably faster time scale than 1-2 ps. In other words, this finding reveals that, from the dynamical point of view, these layers already belong to the bulk liquid phase, and the presence of the interface affects only one single molecular layer in this respect.

### 3.4. Surface orientation

The orientation of a rigid body (e.g., a small molecule) relative to an external direction (e.g., the surface normal) can be completely described by the use of two angular parameters. Therefore, a full description of the orientational statistics of the surface molecules relative to the interface requires the calculation of the bivariate joint distribution of two independent orientational variables [41,42]. We showed that the polar angles $\vartheta$ and $\phi$ of the surface normal vector $\underline{X}$ (pointing, by our convention, from the liquid to the vapour phase) in a local Cartesian frame fixed to the individual molecules is a proper choice of such orientational parameter pair [41,42]. Here we define this local Cartesian frame in the following way. Axis $x$ is the molecular normal axis, axis $y$ is parallel with the line joining the two $CH_3$ groups, and axis $z$ is the main symmetry axis of the molecule, pointing along the C=O double bond from the O to the C atom. The definition of this local Cartesian frame and of the polar angles $\vartheta$ and $\phi$ is illustrated in Figure 5.a. It should be noted that, due to the $C_{2v}$ symmetry of the acetone molecule, the above local Cartesian frame is always chosen in such a way that the inequality

$\phi \leq 90^o$ holds. Further, since $\vartheta$ is the angle of two general spatial vectors, but $\phi$ is formed by two vectors restricted to lay in a given plane (i.e., the *xy* plane of the local frame) by definition, uncorrelated orientation of the molecules with the interface results in a constant probability distribution only if $\cos\vartheta$ and $\phi$ are chosen to be the independent variables [41,42].

It has been shown several times that the local curvature of the surface might have an important influence on the orientation of the molecules [43-48,68,71]. To take this effect also into account, we divided the surface layer into three separate regions, marked by A, B, and C, respectively, in the following way. Regions A and C extend from the *X* points where the density of the surface layer is half of its maximum value towards the vapour and bulk liquid phases, respectively, whereas region B covers the *X* range where the surface layer density exceeds half of its maximum value. The division of the surface layer into regions A, B and C is illustrated in Figure 5.b. According to this definition, region A typically contains the crests of the wavy liquid surface, where the local curvature of the surface is convex, whereas region C covers the troughs of the liquid surface, which are of concave local curvature.

We have calculated the $P(\cos\vartheta,\phi)$ bivariate orientational distribution of the acetone molecules in the first three molecular layers of the liquid surface as well as in the separate regions A, B, and C of the surface layer. The obtained orientational maps (except for those corresponding to the third layer, which, similarly to those of the second layer, turned out to be practically constant) are shown in Figure 6.

As it is seen, the obtained maps show a rather clear orientational structure. This finding is in a marked contrast with our previous result, obtained by investigating the surface orientation of the acetone molecules without performing an intrinsic surface analysis, where we found only very weak orientational preferences [40]. The present results emphasize again the importance of the intrinsic treatment of liquid surfaces in computer simulations, and can, at least partly, resolve the contradiction between our former simulation results and those of Chen et al., who made the surprising claim on the basis of SFG measurements that the surface acetone molecules do not deviate from their preferred alignment by more than $18^o$ [10]. Although we have still obtained a continuous probability distribution for the first molecular layer, which shows high and low probability domains but no completely unpopulated ones, the width of the high probability domain of the orientational map along the $\cos\vartheta$ axis is in the range of about $\pm30-35^o$, much smaller than what was found without using intrinsic surface analysis [40]. On the other hand, the $\phi$ value of the high probability orientations is much less defined.

When looking at the orientational maps obtained in the separate regions A, B, and C of the first molecular layer, a marked difference is seen between regions A and C. Thus, in region A the orientation corresponding to the $\cos\vartheta$ and $\phi$ values of about 0.2 and $0^\circ$, whereas in region C that corresponding to $\cos\vartheta = 0.1$ and $\phi = 90^\circ$ is found to be clearly preferred. These orientations, marked by I and II, respectively, are illustrated in Figure 7.a. These two preferred orientations correspond to rather similar $\cos\vartheta$ values, i.e., similar dipolar alignments of the molecule, in which the C=O double bond (dipolar axis) lays almost parallel with the macroscopic plane of the surface, tilting from it by no more than 10-15$^\circ$, pointing by the O atom slightly inward. Besides a very small additional dipolar tilt, the transition between the two preferred orientations thus corresponds to a $90^\circ$ flip of the molecule around its C=O axis: in orientation I the molecule lays nearly in the macroscopic plane of the surface, whereas in orientation II it stays perpendicular to the surface plane. The difference in the orientational preference of the molecules located in the crests and troughs of the wavy liquid surface emphasizes again the importance of the local curvature of the surface in determining the orientational preferences of the molecules, and can be rationalized by considering that surface acetone molecules are expected to expose their weakly interacting $CH_3$ groups to the vapour phase. Thus, at the tips of the crests both $CH_3$ groups should point to the vapour phase, even if only flatly, in order to keep the polar C=O group safely in the liquid environment. On the other hand, in surface portions of locally concave curvature the molecules can even keep one of their $CH_3$ groups inside the liquid phase by "sacrificing" the other one and sticking it rather straight out to the vapour phase, as illustrated in Fig. 7. However, it is clear that the orientational preferences of the $CH_3$ groups are of secondary importance with respect to that of the C=O groups, i.e., that they prefer to lay almost parallel with the macroscopic surface plane. Therefore, the surface orientation of the acetone molecules is clearly driven by dipolar forces.

The orientational preferences seen in the most populated region of the surface layer, B, is rather similar to that of the entire layer, and shows a combination of the preferences seen in regions A and C. It is also seen that among the two preferred alignments orientation II, i.e., when the acetone molecule stays perpendicular to the macroscopic surface plane, is clearly the dominant one both in region B and in the entire surface layer. The observed dominance of this orientation agrees very well with the experimental finding of Yeh et al. [7], but deviates noticeably from that of Chen et al. [10], who claimed a tilt angle of the C=O bond from the macroscopic surface normal axis of about 60$^\circ$. Finally, all orientational preferences vanish

already in the second molecular layer beneath the surface. It should be noted that orientational preferences can be expected to spread over a few subsurface molecular layers in dipolar liquids due to the electric field caused by the correlated dipolar orientation of the molecules in the surface layer, such as in the case of acetonitrile [45]. However, in the present case the nearly parallel preferred alignment of the molecular dipole vector with the surface plane in the first layer does not impose a considerable electric field along the macroscopic surface normal axis, and hence does not give rise to any preferred molecular orientation from the second molecular layer on.

In bulk liquid acetone nearest neighbour molecules are known to prefer the relative alignment in which their planes are parallel, and dipole vectors are antiparallel with each other [14]. To see if the vicinity of the interface affects this relative orientational preference of the neighbours, we have also calculated the cosine distribution of the angle $\gamma$, formed by two near-neighbouring acetone molecules in the first three subsurface molecular layers as well as in the bulk liquid phase beneath these layers. Two molecules are regarded as near neighbours if the distance of their central C atoms does not exceed 4.5 Å, the value corresponding to one neighbour molecule on average [14]. For comparison, the calculation is repeated with the cut-off value of 5.3 Å, corresponding to the coordination number of 4 [14]. The obtained cosine distributions are shown in Figure 8. As is seen, nearest neighbours prefer antiparallel relative dipolar alignment even at the surface of the liquid phase, and this preference is even stronger in the surface layer than beneath this layer. In this respect, the second layer already behaves again in the same way as the bulk liquid phase, thus, similarly to the roughness and width of the consecutive molecular layers, dynamics of exchange of the molecules, or interfacial orientation, the vicinity of the liquid-vapour interface affects only one molecular layer also in respect of relative orientation of the neighbouring molecules. It is also seen that when, on average, four neighbours of the molecules are considered instead of one, the obtained $P(\cos\gamma)$ distribution becomes rather flat, showing only rather small remains of its features seen with the cut-off value of 4.5 Å. This finding indicates that, similarly to the bulk liquid phase, the observed relative orientational preference affects only the first neighbour of the molecules. The observed interfacial and relative near-neighbour orientational preferences of the surface acetone molecules are illustrated in Figure 7.b.

## 4. Summary and Conclusions

In this paper we presented a detailed computer simulation investigation of the liquid-vapour interface of acetone by means of the ITIM intrinsic surface analysing method. The obtained results clearly demonstrate the importance of identifying the true set of surface molecules, i.e., the ones that are exposed to the opposite phase, and hence analysing the real, molecularly rugged capillary wave corrugated liquid surface rather than a slab of intermediate density parallel with one of the faces of the basic box in computer simulation studies of fluid surfaces. Thus, the present analysis revealed several features of the orientational structure of the acetone surface that were not seen in earlier studies, performed without identifying the intrinsic liquid surface [7,40].

The main orientational preference of the surface acetone molecules relative to the macroscopic plane of the interface is found to be a perpendicular alignment, in which the C=O bond lays almost parallel with the surface plane, pointing very slightly inward by the O atom, and the line connecting the two $CH_3$ groups deviates by only about $5^o$ from the perpendicular alignment. This orientational preference clearly supports the earlier experimental results of Yeh et al. [7] rather than the subsequent claims of Chen et al. [10]. Besides this main orientational preference another alignment, in which the entire acetone molecule lies almost parallel with the macroscopic liquid surface, pointing by about $10^o$ inward by the O atom, and outward by the two $CH_3$ groups, is found to be also preferred, in particular, at the tips of the crests of the wavy liquid surface. Similarly to the bulk liquid phase, two nearest neighbour acetone molecules prefer antiparallel dipolar relative alignment also within the surface layer.

It is also clearly demonstrated that the effect of the vicinity of the vapour phase does not extend beyond the first molecular layer of the liquid phase. Thus, the molecules in the surface layer are somewhat less densely packed than from the second layer on, leading to a broader and rougher surface layer than the consecutive subsurface ones. Orientational preferences of the molecules relative to the interface already vanish in the second subsurface molecular layer, and from the dynamical point of view, again; only the first layer beneath the liquid surface can be distinguished from the bulk liquid phase.

Finally, it should be noted that the two markedly different potential models considered here provided rather similar results in every respect. Therefore, the obtained results can safely

15

be assumed to be free from any arbitrariness due to the particular choice of the potential model used.

**References**

[1]     K. Koga, Y. Kanazawa and H. Shimizu, J. Mol. Spectroscopy **47,** 107 (1973).

[2]     S. M. George, H. Auweter and C. B. Harris, J. Chem. Phys. **73,** 5573 (1980).

[3]     M. A. Villamañán and H. C. Van Ness, J. Chem. Eng. Data **29,** 429 (1984).

[4]     H. Bertagnolli, M. Hoffmann and P. Chieux, Z. Phys. Chem., Neue Folge, **159,** 185 (1988).

[5]     H. Bertagnolli, M. Hoffmann and M. Ostheimer, Z. Phys. Chem., Neue Folge, **165,** 165 (1989).

[6]     K. Mizuno, T. Ochi and Y. Shindo, J. Chem. Phys. **109,** 9502 (1998).

[7]     Y. L. Yeh, C. Zhang, H. Held, A. M. Mebel, X. Wei, S. H. Lin and Y. R. Shen, J. Chem. Phys. **114,** 1837 (2001).

[8]     A. K. Winkler, N. S. Holmes and J. N. Crowley, Phys. Chem. Chem. Phys. **4,** 5270 (2002).

[9]     W. Yi, C. Wang, H. Li and S. Han, J. Chem. Eng. Data **50,** 1837-1840 (2005).

[10]    H. Chen, W. Gan, B. H. Wu, Z. Zhang and H. F. Wang, Chem. Phys. Lett. **408,** 284 (2005).

[11]    S. E. McLain, A. K. Soper and A. Luzar, J. Chem. Phys. **127,** 174515 (2007).

[12]    G. Modla and P. Lang, Ind. Eng. Chem. Res. **49,** 3785 (2010)

[13]    G. J. Evans and M. W. Evans, J. Chem. Soc. Faraday Trans. II **79,** 153 (1983).

[14]    P. Jedlovszky and G. Pálinkás, Mol. Phys. **84,** 217 (1995).

[15]    Yu. G. Bushuev and S. V. Davletbaeva, Russ. Chem. Bulletin **48,** 25 (1999).

[16]    M. G. Martin and M. J. Biddy, Fluid Phase Equilibria **236,** 53 (2005).

[17]    M. H. Ghatee and S. Taslimian, Fluid Phase Equilibria **358,** 226 (2013).

[18]    M. Ferrario, M. Haughney, I. R. McDonald and M. L. Klein, J. Chem. Phys. **93,** 5156 (1990).

[19]    Yu. G. Bushuev and V. P. Korolev, Russ. Chem. Bulletin **47,** 569 (1998).

[20]    L. C. Gomide Freitas, J. M. M. Cordeiro and F. L. L. Garbujo, J. Mol. Liq. **79,** 1 (1999).

[21]    S. Weerasinghe and P. E. Smith, J. Chem. Phys. **118,** 10663 (2003).

[22]    A. Perera and F. Sokolić, J. Chem. Phys. **121,** 11272 (2004).

[23]    P. Jedlovszky and A. Idrissi, J. Chem. Phys. **129,** 164501 (2008).

[24]    P. Jedlovszky, A. Idrissi and Jancsó, J. Chem. Phys. **130,** 124516 (2009).

[25] R. G. Pereyra, M. L. Asar and M. A. Carignano, Chem. Phys. Letters **507,** 240 (2011).

[26] A. Pinke and P. Jedlovszky, J. Phys. Chem. B **116,** 5977 (2012).

[27] R. Semino and D. Laria,. J. Chem. Phys. **136,** 194503 (2012).

[28] D. S. Venables and C. A. Schmuttenmaer, J. Chem. Phys. **113,** 3249 (2000).

[29] G. Kamath, G. Georgiev and J. J. Potoff, J. Phys. Chem. B **109,** 19463 (2005).

[30] A. Perera, L. Zoranić, F. Sokolić and R. Mazighi, J. Mol. Liquids **159,** 52 (2011).

[31] A. Idrissi, I. Vyalov, M. Kiselev and P. Jedlovszky, Phys. Chem. Chem. Phys. **13,** 16272 (2011).

[32] A. Idrissi, K. Polok, W. Gadomski, I. Vyalov, A. Agapov, M. Kiselev, M. Barj and P. Jedlovszky, Phys. Chem. Chem. Phys.**14,** 5979 (2012).

[33] A. Idrissi, K. Polok, M. Barj, B. Marekha, M. Kiselev and P. Jedlovszky, J. Phys. Chem. B **117,** 16157 (2013).

[34] D. R. Wheeler and R. R. Rowley, Mol. Phys. **94,** 555 (1998).

[35] S. Picaud and P. N. M. Hoang, J. Chem. Phys. **112,** 9898 (2000).

[36] G. Hantal, P. Jedlovszky, P. N. M. Hoang and S. Picaud, Phys. Chem. Chem. Phys. **10,** 6369 (2008).

[37] R. Semino, J. Martí, E. Guárdia and D. Laria, J. Chem. Phys. **137,** 194301 (2012).

[38] Y. Rao, Y. S. Tao and H. F. Wang, J. Chem. Phys. **119,** 5226 (2003).

[39] R. Lu, W. Gan, B. H. Wu, H. Chen and H. F. Wang, J. Phys. Chem. B **108,** 7297 (2004).

[40] L. Pártay, P. Jedlovszky and G. Horvai, J. Phys. Chem. B **109,** 12014 (2005).

[41] P. Jedlovszky, Á. Vincze and G. Horvai, J. Chem. Phys. **117,** 2271 (2002).

[42] P. Jedlovszky, Á. Vincze and G. Horvai, Phys. Chem. Chem. Phys. **6,** 1874 (2004).

[43] L. B. Pártay, Gy. Hantal, P. Jedlovszky, Á. Vincze and G. Horvai, J. Comp. Chem. **29,** 945 (2008).

[44] L. B. Pártay, P. Jedlovszky, Á. Vincze and G. Horvai, J. Phys. Chem. B. **112,** 5428 (2008).

[45] L. B. Pártay, G. Horvai and P. Jedlovszky, J. Phys. Chem. C. **113,** 18173 (2009).

[46] Gy. Hantal, M. Darvas, L. B. Pártay, G. Horvai and P. Jedlovszky, J. Phys.: Condens. Matter **22,** 284112 (2010).

[47] K. Pojják, M. Darvas, G. Horvai and P. Jedlovszky, J. Phys. Chem. C. **114,** 12207 (2010).

[48] L. B. Pártay, G. Horvai and P. Jedlovszky, J. Phys. Chem. C. **114,** 21681 (2010).

[49] E. Chacón and P. Tarazona, Phys Rev. Letters **91,** 166103 (2003).

[50] M. Mezei, J. Mol. Graphics Modell. **21,** 463 (2003).

[51] J. Chowdhary and B. M. Ladanyi, J. Phys. Chem. B. **110,** 15442 (2006).

[52] M. Jorge and M. N. D. S. Cordeiro, J. Phys. Chem. C. **111,** 17612 (2007).

[53] A. P. Wilard and D. Chandler, J. Phys. Chem. B. **114,** 1954 (2010).

[54] M. Jorge, P. Jedlovszky and M. N. D. S. Cordeiro, J. Phys. Chem. C. **114,** 11169 (2010).

[55] M. Sega, S. S. Kantorovich, P. Jedlovszky, and M. Jorge, J. Chem. Phys. **138,** 044110 (2013).

[56] N. Foloppe and A. D. MacKerell, Jr., J. Comp. Chem. **21,** 86 (2000).

[57] C. G. Gray and K. E. Gubbins, *Theory of Molecular Fluids*, Vol. 1, Appendix D (Clarendon Press, Oxford, 1984).

[58] S. M. George, H. Auweter and C. B. Harris J. Chem. Phys. **73,** 5573 (1980).

[59] M. P. Allen and D. J. Tildesley, *Computer Simulation of Liquids* (Clarendon Press, Oxford, 1987).

[60] B. Hess, J. Chem. Theory Comput. **4,** 116 (2008).

[61] B. Hess, C. Kutzner, D. van der Spoel and E. Lindahl, J. Chem. Theory Comput. **4,** 435 (2008).

[62] U. Essman, L. Perera, M. L. Berkowitz, T. Darden, H. Lee and L. G. Pedersen, J. Chem. Phys. **103,** 8577 (1995).

[63] S. Nosé, Mol. Phys. **52,** 255 (1984).

[64] W. G. Hoover, Phys. Rev. A **31,** 1695 (1985).

[65] H. J. C. Berendsen, J. P. M. Postma, A. DiNola and J. R. Haak, J. Chem. Phys. **81,** 3684 (1984).

[66] S. A. Levichev, *Oberflächenspannunk, Dichte und Exzessvolumina in binären und ternären Lösungen.* Fiziko-chimičeskie Svojstva Rastvorov (J.80) (Leningradskogo Univ, Leningrad, 1964), pp. 219-226.

[67] J. Chowdhary and B. M. Ladanyi, Phys. Rev. E **77,** 031609 (2008).

[67] M. Darvas, K. Pojják, G. Horvai and P. Jedlovszky, J. Chem. Phys. **132,** 134701 (2010).

[68] M. Darvas, L. B. Pártay, P. Jedlovszky and G. Horvai, J. Mol. Liq. **153,** 88 (2010).

[69] P. Jedlovszky, M. Darvas and G. Horvai, Z. Naturforsch. **68a,** 123 (2013).

[70] P. Jedlovszky, M. Předota and I. Nezbeda, Mol. Phys. **104,** 2465 (2006).

# Tables

Table 1. Interaction parameters of the acetone models used.

| interaction site | $\sigma/\text{Å}$ | $\varepsilon/\text{kJ mol}^{-1}$ | $q/\text{e}$ |
|---|---|---|---|
| TraPPE | | | |
| $CH_3$ | 3.79 | 0.8144 | 0 |
| C | 3.82 | 0.3324 | 0.424 |
| O | 3.05 | 0.6565 | -0.424 |
| CHARMM27 | | | |
| H | 2.352 | 0.0920 | 0.09 |
| $C(H_3)$ | 3.671 | 0.3347 | -0.27 |
| $C(=O)$ | 3.564 | 0.2929 | 0.55 |
| O | 3.029 | 0.5020 | -0.55 |

Table 2. Geometry parameters of the acetone models used.

| bond | bond length (Å) | angle | bond angle (deg) |
|---|---|---|---|
| TraPPE | | | |
| $C$-$CH_3$ | 1.520 | | |
| $C=O$ | 1.229 | | |
| | | $CH_3$-$C$-$CH_3$ | 117.2 |
| | | $CH_3$-$C=O$ | 121.4 |
| CHARMM27 | | | |
| C-H | 1.111 | | |
| C-C | 1.522 | | |
| $C=O$ | 1.230 | | |
| | | H-C-H | 108.4 |
| | | H-C-C | 110.5 |
| | | C-C-C | 116.0 |
| | | $C$-$C=O$ | 122.0 |

Table 3. Characteristics of the consecutive molecular layers of acetone beneath its liquid-vapour interface.

| model | layer | $\delta$/Å | $X_{peak}$/Å | $a$/Å | $\xi$ | $\tau$/ps | |
|---|---|---|---|---|---|---|---|
| | | | | | | continuous | intermittent |
| | first | 6.07 | 48.13 | 3.78 | 0.99 | 16.4 | 27.1 |
| TraPPE | second | 5.84 | 42.73 | 3.53 | 0.84 | 0.8 | 2.1 |
| | third | 5.73 | 37.44 | 3.45 | 0.79 | 0.8 | 2.2 |
| | first | 6.07 | 99.13 | 3.97 | 1.04 | 16.6 | 28.8 |
| CHARMM27 | second | 5.81 | 93.72 | 3.66 | 0.88 | 1.2 | 2.6 |
| | third | 5.67 | 88.38 | 3.52 | 0.83 | 1.0 | 2.3 |

# Figure legend

Figure 1. Equilibrium snapshot of the acetone liquid-vapour interface, as taken out from the simulation performed with the TraPPE model. Molecules belonging to the first, second and third subsurface layers as well as those located beneath these layers are shown by red, green, blue and grey colours, respectively. The C and O atoms of the molecules are marked by darker and lighter shades in every case.

Figure 2. Molecular number density profile of the acetone molecules along the macroscopic surface normal axis $X$ as obtained in the entire system simulated (dashed lines) as well as in the first (circles), second (squares), and third (triangles) molecular layers beneath the liquid surface, as obtained from the simulations performed with the TraPPE (top panel) and CHARMM27 (bottom panel) models. All the profiles shown are symmetrised over the two liquid-vapour interfaces in the basic simulation box.

Figure 3. Average normal distance of two surface points as a function of their lateral distance, as obtained considering the first (black circles), second (red squares), and third (blue triangles) molecular layers of acetone beneath its liquid surface in the simulations performed with the TraPPE (filled symbols) and CHARMM27 (open symbols) potential models. The dashed lines correspond to the fit of equation 4 to the simulated data in the first layer.

Figure 4. Survival probability of the acetone molecules in the first (circles), second (squares), and third (triangles) molecular layer beneath the liquid surface, as obtained from the simulations performed with the TraPPE (left panel) and CHARMM27 (right panel) models. Filled and open symbols correspond to the continuous and intermittent survival probabilities, respectively. To emphasize the exponential decay of the survival probabilities, the plot shows the data on a logarithmic scale.

Figure 5. (a) Definition of the local Cartesian frame fixed to the individual acetone molecules, and of the polar angles $\vartheta$ and $\phi$ of the macroscopic surface normal vector, $\underline{X}$, pointing from the liquid to the vapour phase, in this frame. (b) Definition of the separate regions A, B and C of the surface molecular layer.

Figure 6. Orientational maps of the acetone molecules located in the surface molecular layer of the liquid phase (first column) as well as in its separate regions A (second column), B (third column) and C (fourth column), and in the second subsurface molecular layer (last column), as obtained from the simulations performed with the TraPPE (top row) and CHARMM27 (bottom row) models. The peaks corresponding to the preferred orientations I and II are indicated. Lighter shades of grey correspond to higher probabilities.

Figure 7. (a) Illustration of the preferred surface orientations I and II of the acetone molecules. $\underline{X}$ is the macroscopic surface normal vector pointing from the liquid to the vapour phase. (b) Illustration of the interfacial and near-neighbour relative orientational preferences of the acetone molecules at portions of different local curvature of the liquid surface.

Figure 8. Cosine distribution of the angle $\gamma$, formed by the dipole vector of two neighbouring acetone molecules in the first (red circles), second (green squares) and third (blue triangles) molecular layer beneath the liquid surface as well as in the bulk liquid phase, beneath these layers (black solid lines), as obtained from the simulations performed with the TraPPE (left panel) and CHARMM27 (right panel) models. Filled and open symbols correspond to the near neighbour definitions corresponding to the maximum distance of the two central C atoms of 4.5 Å and 5.3 Å, respectively.
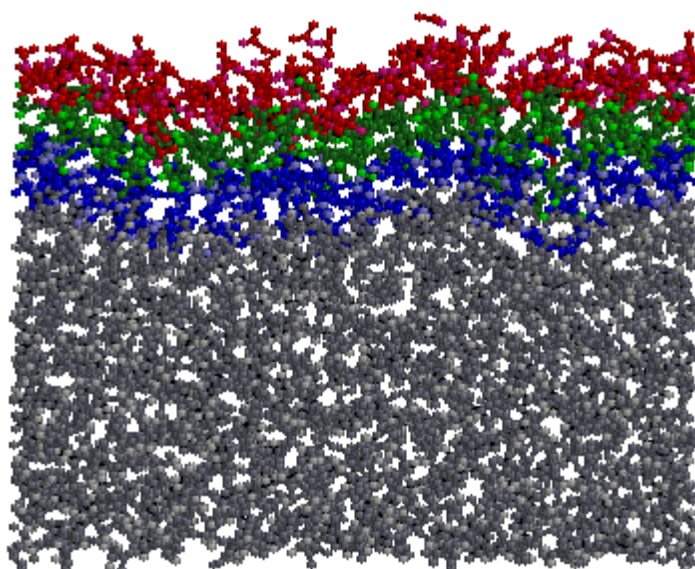
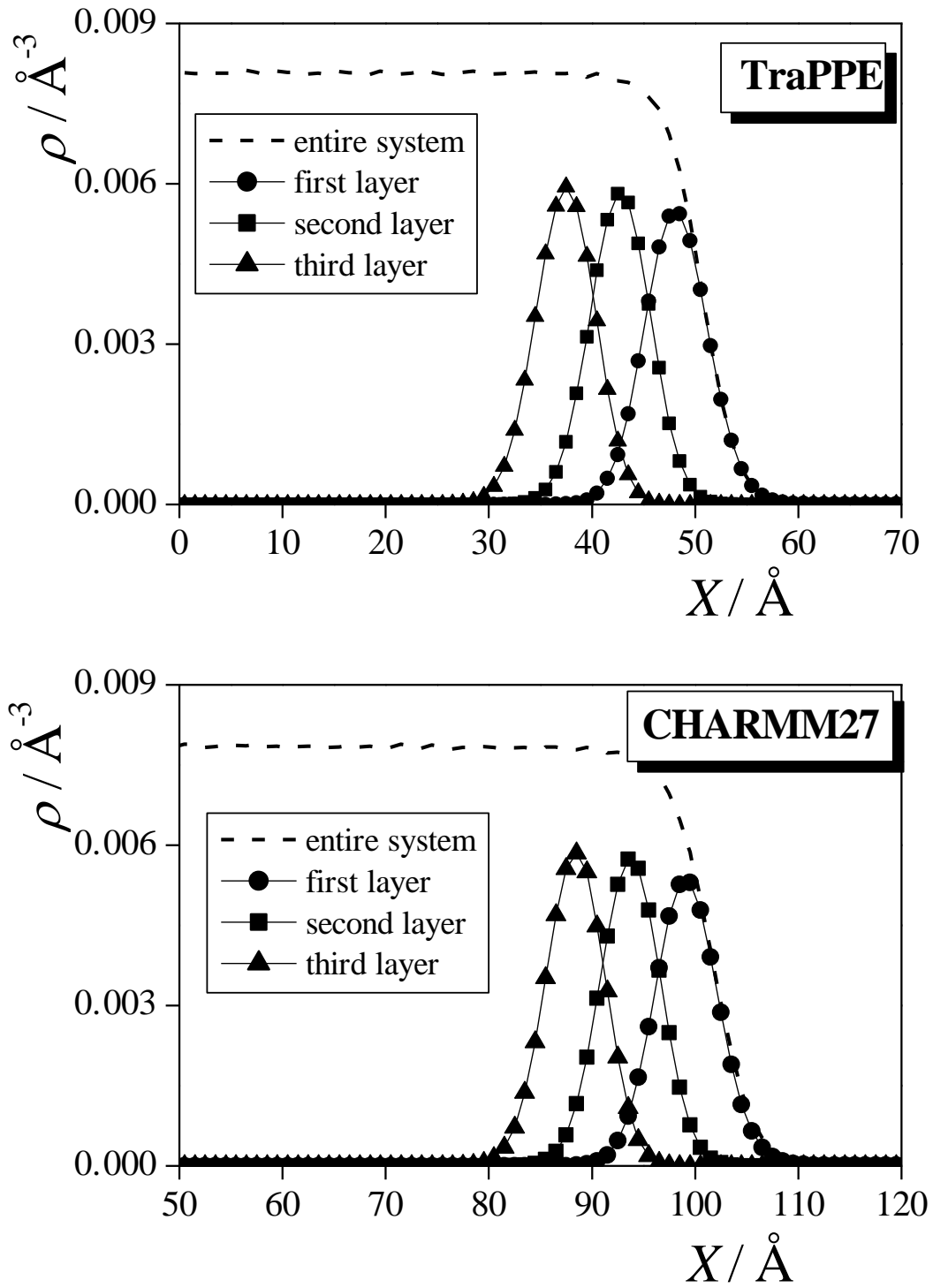Figure 1.

Jedlovszky et al.
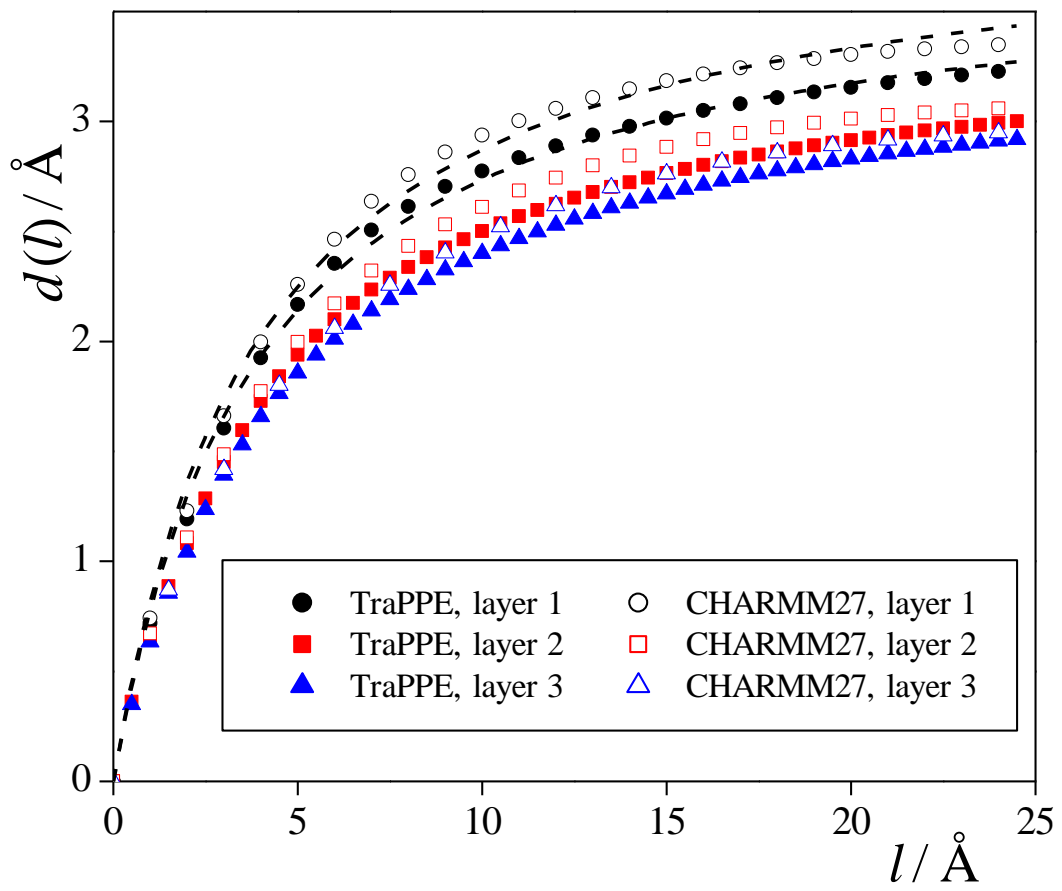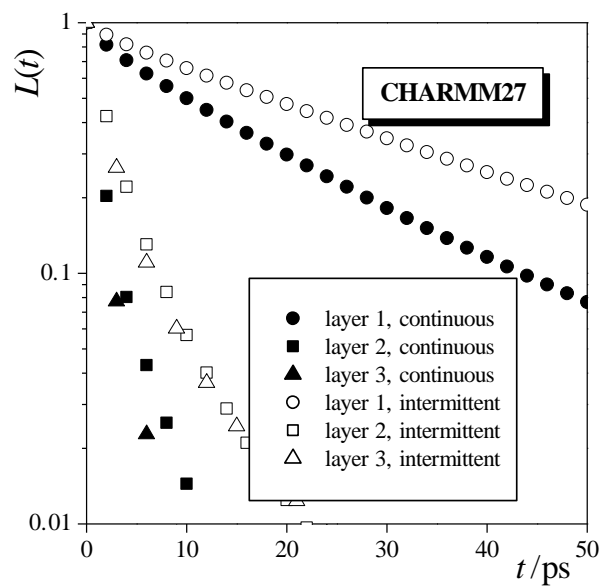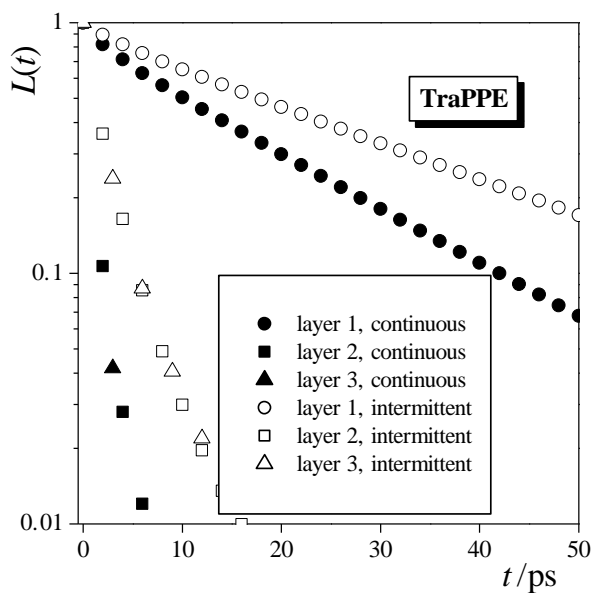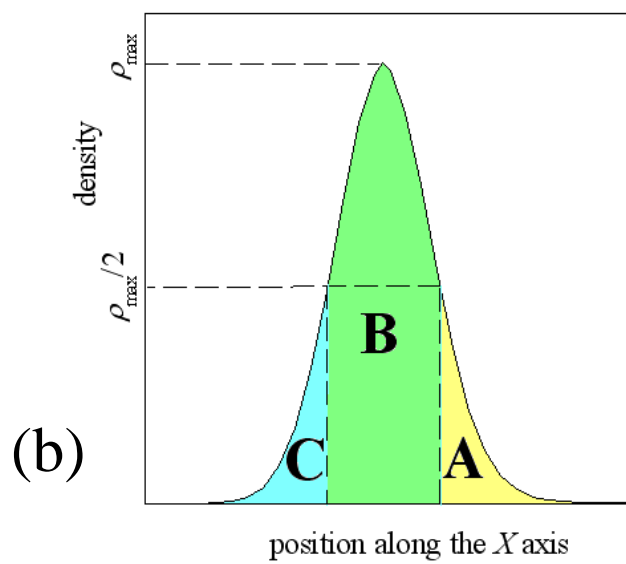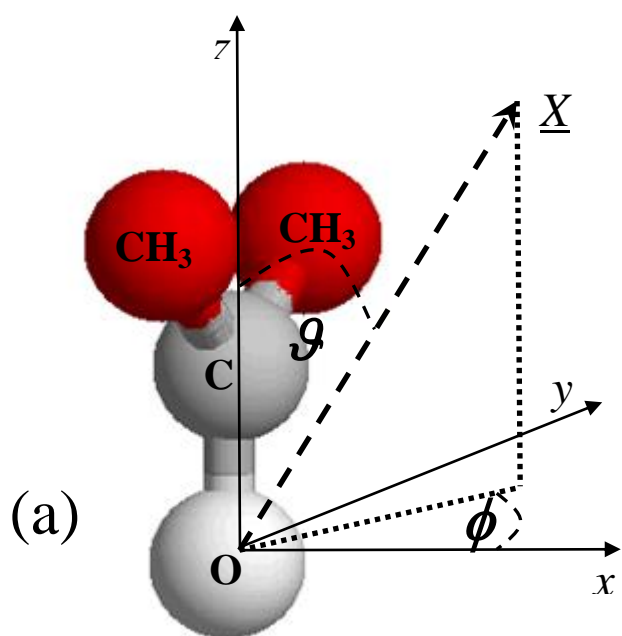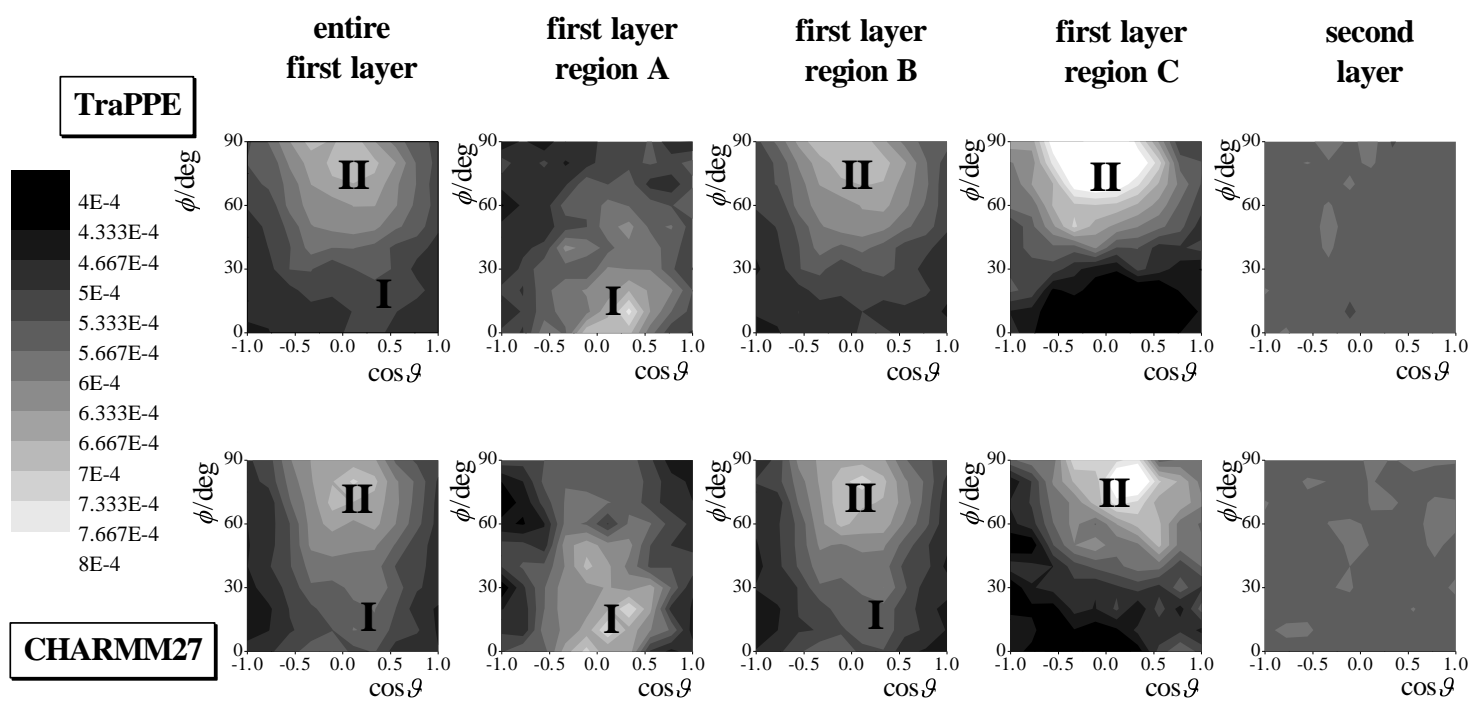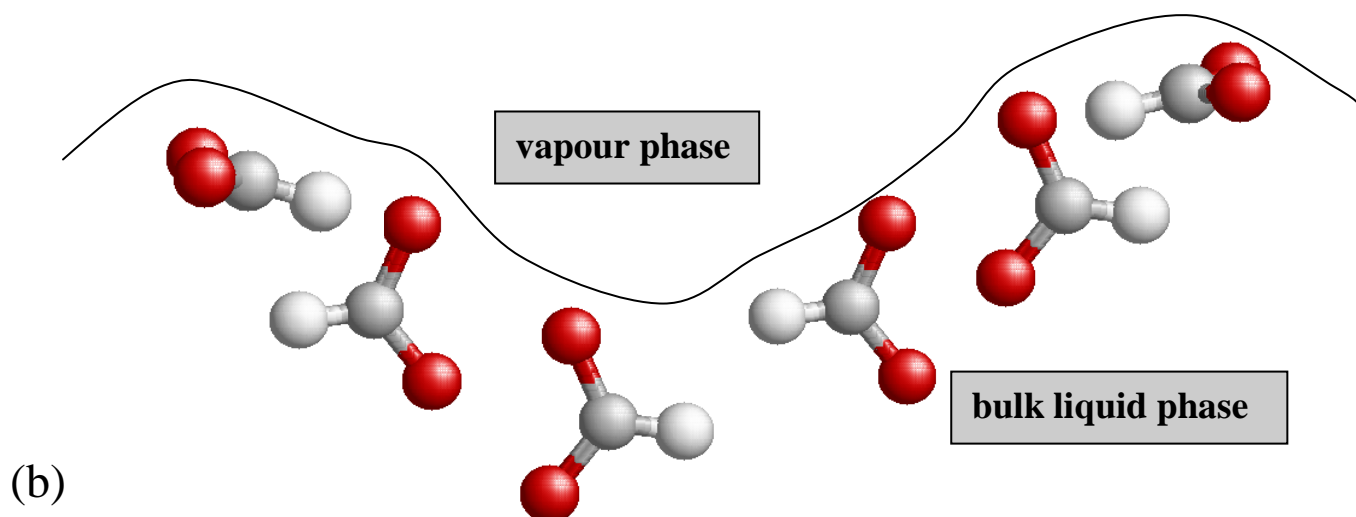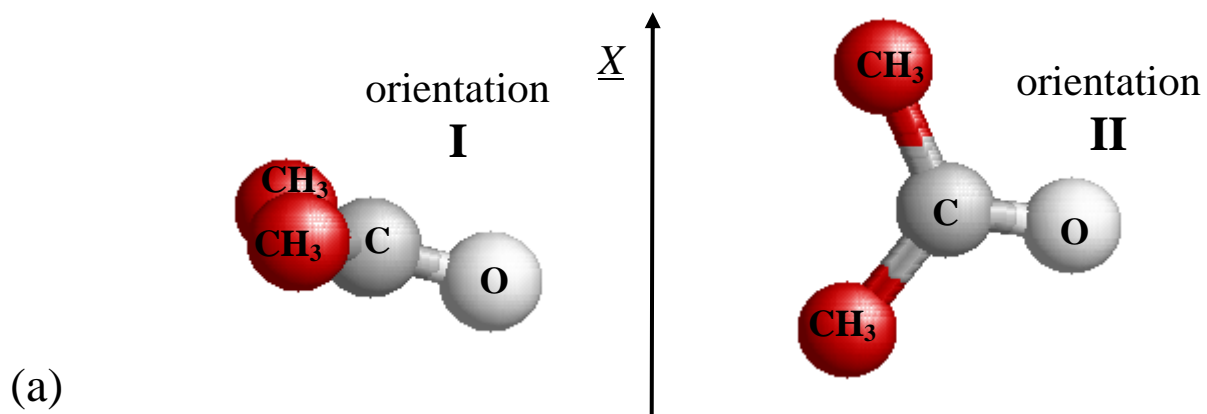
Figure 2.

Jedlovszky et al.

**Figure 3.**

**Jedlovszky et al.**

Figure 4.

Jedlovszky et al.

**Figure 5.**

**Jedlovszky et al.**

(a)



(b)

position along the $X$ axis

**Figure 6.**

**Jedlovszky et al.**

**Figure 7.**

**Jedlovszky et al.**

(a)



(b)

**Figure 8.**

**Jedlovszky et al.**